Rare events in mixed-mode oscillations from weakly coupled lasers

Eusebius J. Doedel[1] and Carlos L. Pando L.[2]
[1]*Department of Computer Science, Concordia University, Montréal, Québec H3G 1M8, Canada*
[2]*Instituto de Física, Benemérita Universidad Autónoma de Puebla, Puebla, Pue. 72570, México*

(Received 14 August 2019; published 11 November 2019)

We study a dynamical system consisting of two mutually coupled molecular lasers, each of which shows mixed-mode oscillations and chaos when uncoupled. The type of coupling, incoherent laser interaction via saturable absorbers is an example of inhibitory nonlinear coupling, which is also found in Hodgkin-Huxley models that describe action potentials in neurons. We have carried out extensive numerical bifurcation analysis and numerical simulations to show that for small-enough coupling, well below the chaotic synchronization threshold, the presence of distinctive resonances in a symmetric mirror configuration of the system generates a type of rare events characterized by very small amplitudes. When this symmetry is broken by introducing a relatively small difference between the lasers pump parameters near an in-phase Hopf bifurcation, we observe extreme rare events (rogue waves) in one of the lasers. In this case the outliers deviate from power-law distributions and are reminiscent of those known as dragon kings. We consider the conditions for both types of rare events to occur, their origin, as well as relevant statistical features.

DOI: 10.1103/PhysRevE.100.052204

I. INTRODUCTION

Despite the rather large amount of data found in nature, qualitatively different events of interest are often quite rare, i.e., rare events. Their frequency depends on the particular field of study [1], such as in flow cytometry, where rare-event analysis typically refers to detection of episodes that happen at a frequency of 0.1% percent or even much less, such as at 1 in 10^7 occurrences (0.00001%) for tumor cells [2]. In the case of extraordinary events, the celebrated physicist Freeman Dyson recounts that Nikolai Kardashev, a renowned astrophysicist, predicted that if we ever observe an alien society, it should belong to type 2 or type 3 civilizations, even if these events are as rare as one in a million, a *black swan*. We have not yet achieved type 1 status [3], where the status depends on the amount of energy a society is able to control. In the context of popular narrative a black swan is an unpredictable episode which is not expected and has potentially severe consequences [4].

There is a large literature related to the statistics of rare events of small, intermediate, and relatively large amplitude, whose goal is the study of the associated probability distribution functions (PDF). Typically, frequency-size distributions or cumulative distributions with heavy-tailed features disclose rare events whose properties in general differ from those of the PDF core in a significant way. As a result, their prediction typically has been limited to the expected occurrence of an event within a range of values [5]. This happens as many issues are still unclear, such as the mechanisms related to their onset, a topic of current interest. The study of extreme rare events, also known as rogue waves, is an important subject in the physical sciences, such as in hydrodynamics, e.g., turbulence, hurricanes, and tsunamis, and in geosciences, e.g., earthquakes, floods, and landslides [5,6]. For instance, recent research on the temporal variability of individual rogue waves in coastal environments showed that their rate of occurrence displays a decreasing trend; however, their seasonal severity is becoming more critical, resulting in eventual serious hazards [7].

Within the context of our model, the study of extreme rare events in quantum and nonlinear optics became more active after the work of Solli *et al.* [8]. Although a unique definition of a rogue wave (RW) does not exist, there are four important features within the context of optical pulses: (i) the magnitude of their intensity, much larger than the average of nearby pulses; (ii) fast rise, (iii) fast fall, and (iv) the rate of occurrence, which is described by non-Gaussian and long-tailed PDFs [9,10]. However, suitable PDFs may deviate from power-law or Levy distributions [11]. As for low-dimensional chaotic optical oscillators, crises have been found as possible mechanisms for the onset of rare events [12].

The purpose of this paper is to show that rare events of both very small and very large amplitude, being outliers on a suitable scale, may occur in an autonomous system of mutually coupled lasers. We study their onset, dynamics, and conditions to observe them. Outliers display statistical properties that differ from those within the PDF core in a significant way [13].

In our model for the laser system the coupling parameter range is weak, well below the threshold for chaotic synchronization. Synchronization has been widely studied and qualitatively refers to a mechanism by which rhythms of interacting oscillators become and remain adjusted [14,15]. Theoretically and experimentally [16–21] it was shown that chaotic systems under appropriate mutual interactions are capable of exhibiting different kinds of synchronization behavior. Several types of chaotic synchronization have been identified, such as complete synchronization, generalized synchronization, phase synchronization, lag synchronization, anticipated synchronization, crowd synchrony [22], and synchronization in complex networks [15]. Just before the onset

of chaotic synchronization a phenomenon known as *bubbling* has been found, which is a form of intermittency caused by riddled basins of attraction near the synchronized chaotic state [23–25]. The range of coupling parameters considered in our model is even smaller than that to observe bubbling phenomena.

In the present study we consider two qualitative different settings for our laser system, where we show evidence of rare events and discuss their origin when in both cases the coupling parameter is small enough. In the first case the coupled lasers have a symmetric configuration, while in the second a suitable parameter, the laser pump, in one of the laser oscillators brings about an asymmetry near a Hopf bifurcation. We discuss the origin of the observed rare events in the time series on the basis of a bifurcation analysis of relevant families of the resonances as suitable parameters are changed.

An important feature of our coupled system is the presence of complex mixed mode oscillations. Mixed mode oscillations (MMO) display several time scales and are the subject of substantial current research in several experimental systems [26–28], where they refer to cycles formed by a number of spikes followed by several small-amplitude oscillations. In the laser dynamical regime under study, Q-switching operation, a saturable absorber element prevents the energy inside the system to be released fast enough and suitably stores it before it is freed as an optical pulse [29–31]. The coupling mechanism in our system, which is induced via saturable absorbers, has been studied both theoretically and experimentally in coupled CO_2 lasers [32–34].

This article is organized as follows. In Sec. II we introduce and discuss the coupled laser model, while in Sec. III we examine rare events of very small amplitude which arise in numerical simulations when the coupled laser oscillators are identical. In the next section we consider a bifurcation analysis of the resonances which generate these rare events. This consists of one- and two-parameter bifurcation diagrams for the laser pump and coupling strength, as obtained by a numerical continuation analysis with the package AUTO [35]. In Sec. V along similar lines we deal with the case of an asymmetrical laser configuration where rogue waves may emerge near a Hopf bifurcation. Our conclusions and a discussion are presented in Sec. VI.

II. THE MODEL

We describe a model for bidirectional coupling in a pair of class-B single-mode Q-switched lasers: two mutually coupled CO_2 lasers via their saturable absorbers (LSA). The uncoupled laser case is described by a model known as the four-level model [36,37]. The CO_2 LSA is a relevant system of class-B lasers and its giant laser spikes are known as passive Q-switching self-pulsations, which are a good example of MMOs. The scope of the dynamical phenomenology of the CO_2 LSA made it an interesting object for study in nonlinear dynamics [38–43]. We consider a special type of coupling of Q-switched lasers, namely optical coupling via saturable absorbers, which is also a form of incoherent coupling. This coupling scheme between these laser systems has been implemented both theoretically and experimentally in CO_2 lasers [32–34].

Each of the two laser devices is described by a reduced four-level model [36,37] and the mutual coupling is implemented through a fast saturable absorber. This system is modeled in Eq. (1), where I_i stands for the field intensities within the laser cavities, the fast variables, and v_i and w_i denote the effective populations of the lower and upper (excited) rotational energy levels in the gain medium, respectively, where $i = 1, 2$ is the laser oscillator label. Here v_i and w_i are the slow variables. Q_i is the incoherent pump induced by the excitation current in the gain media, and z is the effective number of reservoir rotational levels in each vibrational band in the gain medium. The last term in the equations for I_i stands for the saturable absorber, the parameter α is proportional to the density of absorber molecules and β is known as the saturability [36,37], while c is the coupling constant. The vibrational relaxation rates for the upper (excited) and lower vibrational levels in the CO_2 molecules are called γ_2 and γ_1, respectively,

$$\begin{aligned}
\frac{dI_1}{dt} &= I_1\left\{-1+\frac{(z+1)\Omega_1}{z}(w_1-v_1)\right.\\
&\quad\left.-\frac{\alpha}{1+2\beta[(1-c)I_1+cI_2]}\right\},\\
\frac{dv_1}{dt} &= \Omega_1 I_1(w_1-v_1)-\gamma_1 v_1\,,\\
\frac{dw_1}{dt} &= \Omega_1 I_1(v_1-w_1)-\gamma_2 w_1+z\gamma_2 Q_1\,,\\
\frac{dI_2}{dt} &= I_2\left\{-1+\frac{(z+1)\Omega_2}{z}(w_2-v_2)\right.\\
&\quad\left.-\frac{\alpha}{1+2\beta[(1-c)I_2+cI_1]}\right\},\\
\frac{dv_2}{dt} &= \Omega_2 I_2(w_2-v_2)-\gamma_1 v_2\,,\\
\frac{dw_2}{dt} &= \Omega_2 I_2(v_2-w_2)-\gamma_2 w_2+z\gamma_2 Q_2\,.
\end{aligned} \tag{1}$$

Also in Eq. (1), we have defined

$$\Omega_i=\frac{z+1}{(z+1)^2+2zI_i/\gamma_{R'}},\ i=1,2,$$

where γ_R' stands for the characteristic rotational relaxation rates of CO_2 molecules within the same vibrational band [36,37]. Moreover, the saturable absorber is assumed to be fast and identical in both lasers. The fixed parameter values are $\alpha = 0.75$, $\gamma_R' = 0.2205$, $\gamma_1 = 0.0252$, $\gamma_2 = 0.00315$, $z = 10$, and $\beta = 200$, while the parameters Q_1, Q_2 and the coupling strength c are allowed to change. All relaxation parameters, the time t, and the parameter α have been renormalized through division by the photon lifetime in the laser cavity [36,44].

Equation (1) and related CO_2 LSA models for the case of uncoupled lasers, where $c = 0$, have been studied to a good extent. In this case qualitatively relevant features remain the same, such as the isolas and period-adding cascades [44]. For a similar model of two unidirectionally and two mutually absorber-coupled Q-switched CO_2 lasers we have shown that there are isolas with in-phase and phase-locked periodic

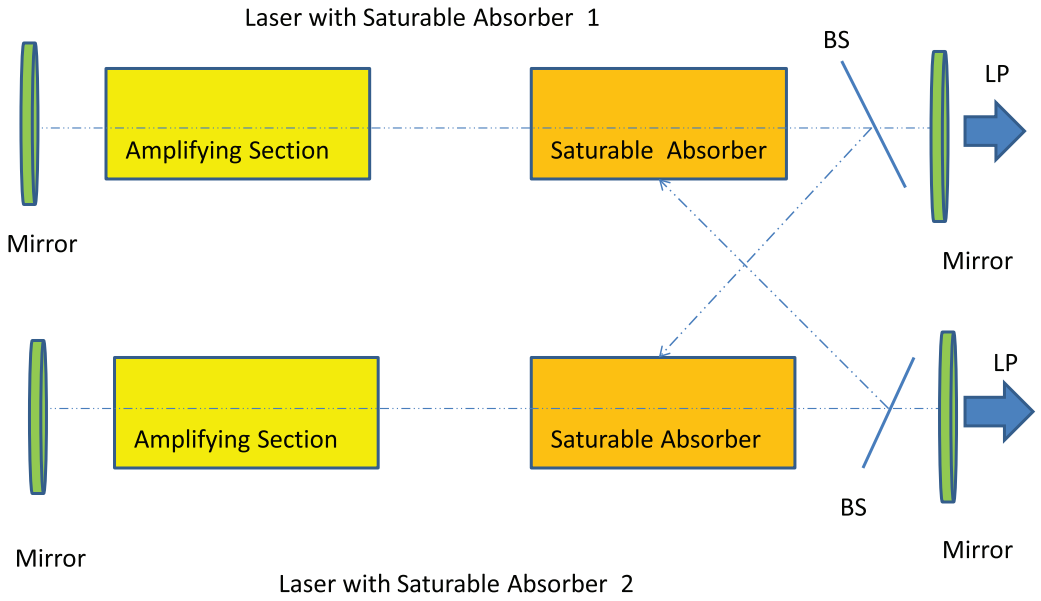

FIG. 1. Diagram which illustrates Eq. (1). Here the dashed blue lines and labels BS and LP denote the laser beam intensities I_1 and I_2, beam splitter, and laser pulse output, respectively. Both laser systems are mutually coupled through their saturable absorbers.

solutions [45,46], where the case of chaos synchronization was also considered. It is worthwhile mentioning that isolas do not exist in a basic two-level rate-equation model [47].

The diagram in Fig. 1 qualitatively illustrates an experimental set up for Eq. (1). This schematic has the key ingredients of the model, such as Eq. (1), and has been studied both experimentally and theoretically within the context of chaotic synchronization by Sugawara *et al.* for the case of unidirectionally coupled Q-switched CO_2 lasers [33]. Other experimental configurations have been considered, such as coupling through a common saturable absorber [32,34], where resonances and synchronization effects were studied for this strongly asymmetric laser system. Our study, however, focuses likewise on the general problem where mirror symmetry and symmetry breaking induced by small defects are features of the dynamical system. As a result we have chosen the bidirectional weakly coupled case for the laser system studied in Ref. [33].

III. CASE I: RARE EVENTS IN SYMMETRICALLY PUMPED LASER OSCILLATORS

For convenience of presentation this section is divided into two subsections. In the first we consider the rare events of the system and the related statistics, while in the second subsection we investigate the resonances embedded in the time series for the laser intensities $I_{1,2}$. This will be valuable in Sec. IV to explain the origin of these rare events by considering different families of periodic solutions of Eq. (1) and their bifurcations, as obtained by numerical continuation analysis [35].

A. Extremely small amplitude rare events in the time series

To clearly identify the extremely small amplitude rare events (ESARE), we first plot the typical behavior of the laser intensities. Figure 2 gives an idea of the characteristic oscillations in $I_{1,2}$ when both laser oscilators are identical, where the largest spikes and their following undulations are also shown on a logarithmic scale. The coupling parameter is $c = 0.002 \ll c_{\text{sync}}$, where $c_{\text{sync}} \approx 0.05$ is the coupling near which complete synchronization occurs. The ESARE are shown in the time interval of Fig. 3, where the local maxima are near $\log I_{1,2} \equiv \ln I_{1,2} \approx -46$. One such local maximum can be seen in Figure 3(b). Figure 3(a) suggests that when some ESARE builds up, there is a nonzero probability for the occurrence of another ESARE soon after in the time series, as will be discussed next. The time series may be viewed as well as a stationary process [48].

To have statistical estimates of ESARE, we first obtain a time series from a Poincaré section by means of finding consecutive maxima of $\log I_1$, which statistically is the same as $\log I_2$ due to the mirror symmetry and the stationarity of

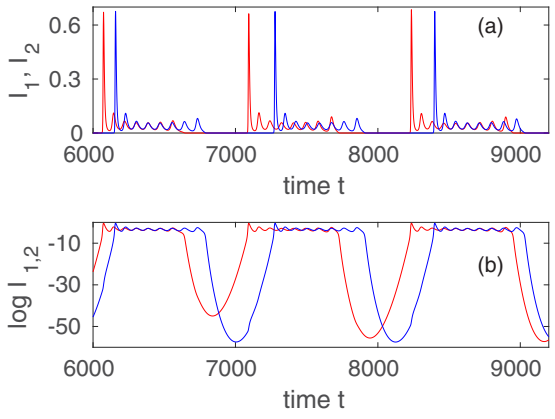

FIG. 2. (a) Time dependence for $I_{1,2}$ (red and blue) in Eq. (1) for the coupling constant $c = 0.002$ and pump parameter $Q = 2.26$. (b) Same time evolution in (a) for $\log I_{1,2} \equiv \ln I_{1,2}$. The value $c = 0.002$ is much smaller than the synchronization threshold $c_{\text{sync}} \approx 0.05$. The coupled LSA have mirror symmetry. Here log denotes natural logarithm.

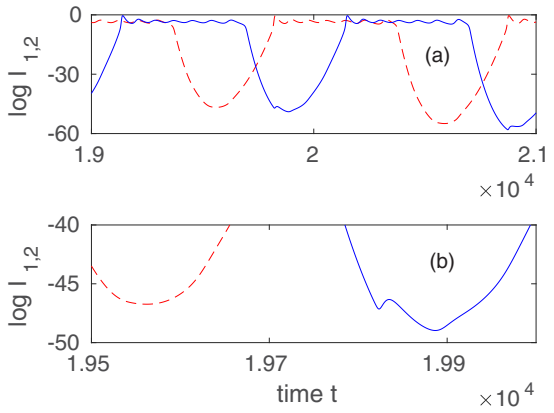

FIG. 3. (a) Time evolution for $\log I_{1,2}$ (red and blue) in Eq. (1) when two rare events occur for the coupling constant $c = 0.002$ and pump parameter $Q = 2.26$. See the local maxima near $\log I_{1,2} \approx -46$. (b) A close-up of (a).

the time series. Figure 4 shows that for very weak coupling constants, such as $c = 0.00002$, and pump parameter $Q = 2.26$, no rare events were observed in 10^5 consecutive iterates in the time series. Still for weak coupling constants, but above $c = 0.00002$, ESARE emerge as seen in the lower panel of Fig. 4, where a few events are observed near $\log I_{1,2} \approx -50$. The rate R of occurrence of ESARE may be controlled through the coupling constant c as indicated in Fig. 5(b), where the number of rare events is counted within 10^5 consecutive iterates of the Poincaré section. In Fig. 5(a) the average frequency ν is defined as the number of maxima occurring over a discrete time T ($T \sim 10^5$), as obtained for a system of coupled lasers [49], while the number of ESARE in these time series, R, is roughly less than 400 during T. As seen in the upper panel of this figure, ν has small fluctuations around a mean value. In all time series in this section we consider coupling parameters c when the growth of ESARE has a positive slope, that is when $c \ll 0.001$. For $c \approx 0.001$

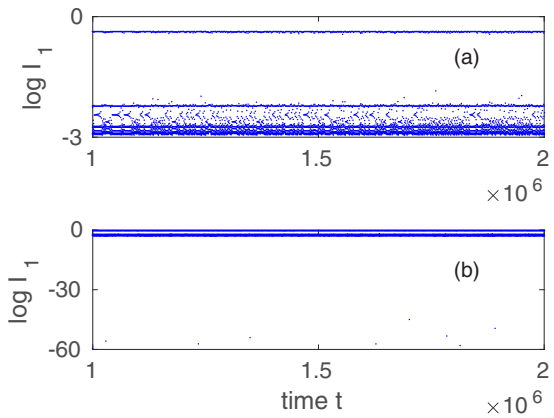

FIG. 4. (a) Time series for the Poincaré section from I_1 in Eq. (1) for the coupling constant $c = 0.00002$ and pump parameter $Q = Q_1 = Q_2 = 2.26$, where no rare events were observed in 10^5 iterates. (b) Same as (a) but for the coupling constant $c = 0.0005$, where a few rare events are observed near $\log I_{1,2} \equiv \ln I_{1,2} \approx -50$. Here log denotes natural logarithm.

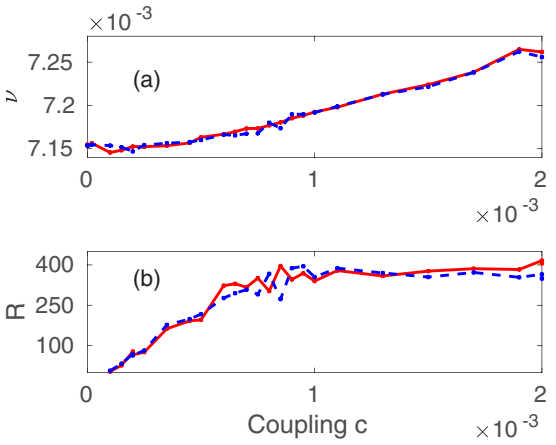

FIG. 5. (a) Average frequency ν versus coupling parameter c for the pump parameter $Q = 2.26$. (b) Number of ESARE, R, versus coupling parameter c from the Poincaré section time series for $\log I_1$ (red) and $\log I_2$ (blue) over $T \approx 10^5$ successive iterates. The coupled LSA have mirror symmetry.

or larger other effects (new resonances) may come into play as R saturates as seen in the plateau of Fig. 5(b).

As for the statistics of ESARE, which emerge within events of small, intermediate, and large amplitude, we study their associated PDF, whose properties differ from those of the PDF core in a significant way. This is shown in Fig. 6, where the PDF cores for $c = 0$ and $c = 0.0005$ are displayed in Figs. 6(a) and 6(b) respectively, where in Fig. 6(b) the cumulative probability is close to 1. Both look similar, as the coupling is weak enough compared to c_{sync}. In contrast to the PDF core, that for the outliers when $c = 0.0005$ suggests heavy-tailed features as shown in Fig. 6(c).

In the interspike time intervals between small, intermediate (undulations), and large amplitude spikes, on the one hand, and in the discrete time series for the interspike time intervals between successive ESARE, on the other, the peculiar features

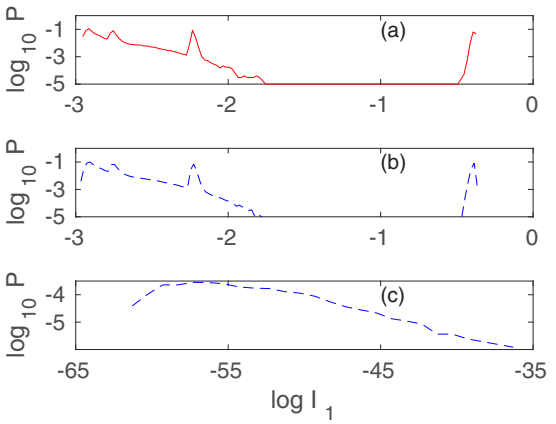

FIG. 6. (a) $\log_{10} P$, where P stands for the PDF for $\log I_1$ when the coupling $c = 0$. (b) $\log_{10} P$ for $\log I_1$ when $c = 0.0005$ and $Q = Q_1 = Q_2 = 2.26$ for the interval $-3 \leqslant \log I_1 \leqslant 0$. (c) Same as (b) but for the interval $-65 \leqslant \log I_1 \leqslant -35$. Within the interval $-35 \leqslant \log I_1 \leqslant -3$ the PDF P is negligible. The times series contains 10^6 iterates of the Poincaré section.

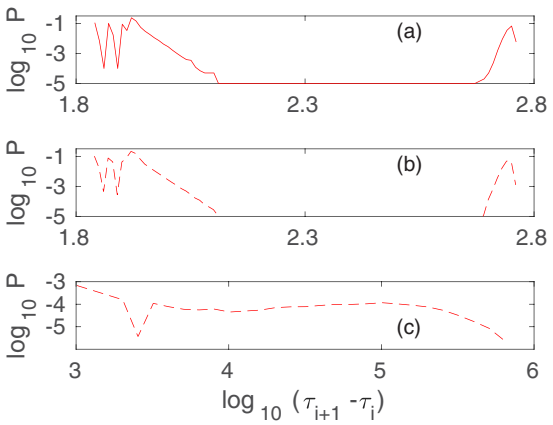

FIG. 7. (a) $\log_{10} P$, where P stands for the PDF, for $\log_{10}(\tau_{i+1} - \tau_i)$ when the coupling $c = 0$. τ_i is the time at the Poincaré section for $\log I_1$. (b) Same as (a) when $c = 0.0005$. (c) $\log_{10} P$ versus $\log_{10}(\tau_{i+1} - \tau_i)$, where τ_i is now the time at the Poincaré section when ESARE occurs.

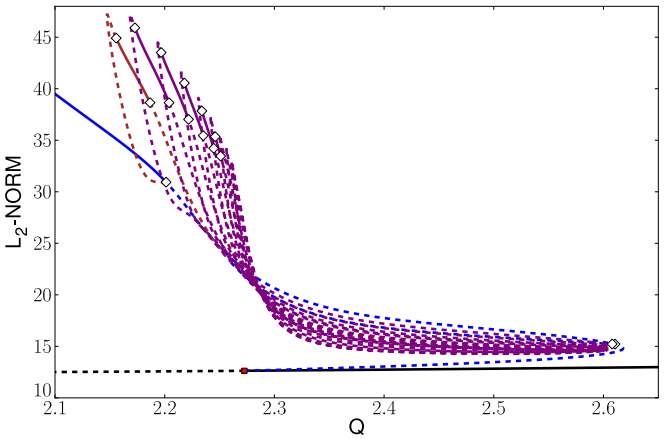

FIG. 8. A bifurcation diagram for the single laser, showing the norm of the periodic solutions, as defined by Eq. (2), versus the pump parameter Q. Shown are the stationary family (bottom) and the primary periodic family that emanates from the Hopf point (small solid square). The curves near the top-left correspond, from left to right, to the primary periodic family, a period-doubled family, and the isolas $\hat{I}_{03}$, $\hat{I}_{04}$, $\hat{I}_{05}$, …, $\hat{I}_{10}$. Period-doubling bifurcations are represented by open diamonds.

for the outliers can be observed. This is shown in Fig. 7, where the PDF for $c = 0$ and $c = 0.0005$ are displayed in Figs. 7(a) and 7(b) respectively. Both PDF look similar as the coupling c is weak enough compared to c_{sync}. In Figs. 7(a) and 7(b) the maxima on the left, where $\log_{10}(\tau_{i+1} - \tau_i) \sim 1.8$, are related to the interspike intervals between successive undulations, while those on the right, where $\log_{10}(\tau_{i+1} - \tau_i) \sim 2.7$, are related to undulations and large spikes. In contrast, the PDF for successive ESARE when $c = 0.0005$ suggests a persistence in time of ESARE near $\log_{10}(\tau_{i+1} - \tau_i) \sim 3$. After a PDF drop follows a relative flat distribution for almost two orders of magnitude for $\tau_{i+1} - \tau_i$, as shown in Fig. 7(c).

B. Resonances embedded in the Poincaré section time series

To have an idea of the resonances which the trajectory visits, as observed in the time series of the Poincaré section, we need to identify its components and understand how often these are visited. This will be useful to search for the appropriate resonances in the coupled lasers system in the numerical continuation study of the next subsection. The uncoupled case bifurcation diagram, $c = 0$, turns out to be very useful to detect the resonance components that arise in the time series for small coupling c.

The bifurcation diagram for the single laser in Fig. 8 includes families of periodic orbits that connect smoothly to themselves and are isolated from the basic solution families. Such families are commonly referred to as *isolas*. Specifically, Fig. 8 includes the first eight isolas, superimposed on the basic solution families. The isolas are colored purple and will be referred to as $\hat{I}_{03}$, $\hat{I}_{04}$, $\hat{I}_{05}$, etc. There may in fact be an infinite sequence of such isolas. The primary family (blue) and the period-doubled family (brown) contain a region of stability. The isolas $\hat{I}_{03}$–$\hat{I}_{07}$ also contain a region of stability, bordered by period-doubling bifurcations (open diamonds). For the current value of β, namely $\beta = 200$, the subsequent isolas, $\hat{I}_{08}, \hat{I}_{09}, \ldots$, do not contain a region of stability. The choice of norm as vertical axis is mostly because it generally gives reasonably clear diagrams. This norm is in fact the integral L_2 norm of the solutions over a scaled time interval [0,1], including all three solution components, i.e., the norm is defined as

$$\text{norm} = \left\{ \int_0^1 [\log I(t)]^2 + v(t)^2 + w(t)^2 \, dt \right\}^{\frac{1}{2}}. \qquad (2)$$

The L_2 norm, as defined by Eq. (2), is a suitable measure or gauge for periodic orbits. We note that in our figures the choice of the solution measure is mostly given by the clarity of the bifurcation diagrams it produces. Other possible measures are $|\log I(t)|$ or the period T of the periodic orbit [44]. The period T may be useful as it carries information about the time unit, which in Eq. (1) is the photon lifetime in the laser cavity [44].

The rate that the trajectory for the single laser ($c = 0$) visits different UPOs of Fig. 8 are shown in the histogram of Fig. 9(a), where it is clear that the most visited UPOs are those with $m = 8, 9$ maxima, or $m - 1$ undulations and m maxima between two interspike intervals in the trajectory. There is a consistent correlation between this PDF and the Floquet multipliers Λ_i, $i = 1, 2$ for a given UPO. Indeed, the smallest absolute values for the expanding Floquet multipliers are precisely for UPOs with $m = 8, 9$ maxima. Correspondingly these UPOs have the largest contractive rates as shown by the parameter $\lambda_1 + \lambda_2 \equiv \log_{10} |\Lambda_1 \Lambda_2|$, as shown in the lower panel of Fig. 9.

For nonzero coupling parameter, $0 < c \ll c_{\text{sync}} \sim 0.05$, as discussed in the text for Fig. 5, the trajectory becomes more complex, but still shadows to a good extent UPOs similar to those of Fig. 8. Proceeding as we did for the time series when $c = 0$, now the resonances involve new UPOs as c is slightly above zero. Their new features, such as their folds, quantitatively and qualitatively will be discussed in the next section. The presence of qualitatively new UPOs is already visible in the histogram of Fig. 10, e.g., UPOs with more or

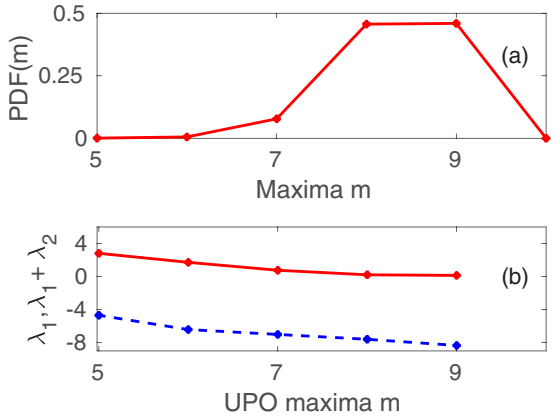

FIG. 9. (a) PDF for the number of times m maxima ($m-1$ undulations) arise between two interspike intervals in the time series. Here $Q = Q_1 = Q_2 = 2.26$ and the coupling $c = 0$. (b) $\lambda_i \equiv \log_{10} | \Lambda_i |$, $i = 1, 2$, where Λ_i are the Floquet multipliers corresponding to the unstable periodic orbit (UPO) with m maxima. In (b) the dashed line stands for the contractive rates.

less undulations, where as a reference we have inserted the PDF for $c = 0$ using red lines, in the four panels where PDF for different values of c are plotted. The above information, obtained from a single time series for I_1, suggests that the most visited resonances are those of the type $N : M$, where $N : M$ is $8 : 8, 9 : 9, 8 : 9, 7 : 9$, etc., as the coupled system is symmetric and the laser oscillators behave to good extent as independent.

In the present study we note that a resonance $N : M$ refers to a periodic orbit for the coupled system, where a laser oscillator shows N oscillations or maxima while the other oscillator displays M maxima for nonzero coupling c during the complete period. In the next section we show how to generate these resonances.

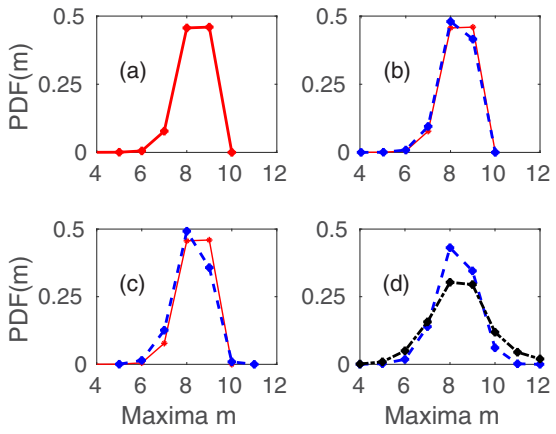

FIG. 10. PDF for the number of times m maxima ($m-1$ undulations) arise between two interspike intervals in the time series. Here $Q = Q_1 = Q_2 = 2.26$ and the coupling parameter c is changed. (a) Coupling parameter $c = 0$ (red). (b) Same as (a) but for $c = 0.0002$ (blue) and $c = 0$ (red). (c) Same as (b) but for $c = 0.00075$ (blue) and $c = 0$ (red). (d) Same as (b) but for $c = 0.0015$ (blue) and $c = 0.003$ (black). In panels (a),(b) and (c) the continuous lines stands for $c = 0$. In panel (d) the largest maximum corresponds to $c = 0.0015$.

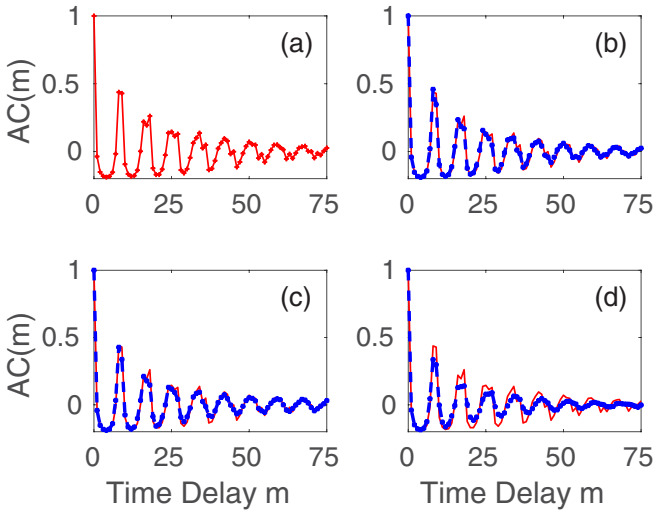

FIG. 11. The AC for the time series of I_1 from the Poincaré section versus the discrete time delay m for different couplings c, when $Q = Q_1 = Q_2 = 2.26$. (a) Coupling constant $c = 0$ (red). (b) Same as (a) but for $c = 0.0005$ (blue) and $c = 0$ (red). (c) Same as (b) but for $c = 0.001$ (blue) and $c = 0$ (red). (d) Same as (b) but for $c = 0.002$ (blue) and $c = 0$ (red). The continuous lines stands for $c = 0$.

By calculating the coherence length for the discrete time series of I_1 via the autocorrelation function (AC) in Fig. 11, we realize that we can assess the degree of persistence of the trajectory near some UPOs. We observe that there is a match between the largest probabilities for UPOs with $m = 8, 9$ in the histograms of Fig. 10 and consecutive maxima of the AC, which qualitatively repeat every time there is a delay difference $\Delta m \approx 8$. In particular, once a laser oscillator visits a nearby UPO with $m = 8$, it is prone to repeat this kind of oscillation L times. This we call *laminar phase* and is characterized by a probability $P(L)$ which depends on the length L of the laminar phase, i.e., $L = 3$ for UPOs with $m = 8$ stands for a trajectory portion visiting three consecutive UPOs with $m = 8$ for the laser oscillator I_1. The dependence of $P(L)$ on L is decreasing exponentially for several coupling parameters c as shown in Fig. 12. For coupling parameters $c \leqslant 0.001$ we can see that the average slopes in Fig. 12 slightly change; however, for $c \geqslant 0.001$ these changes are more pronounced. The slight change of the slopes for the laminar phases L occurs when the growth of the number of ESARE R changes gradually for $c \leqslant 0.001$, i.e., before R saturates, as shown in Fig. 5.

Complementary information can be gained when analyzing the cross-correlation function (CC) for a dual time series [48], consisting of data at the Poincaré section for the maxima of I_1 and the related value of I_2, versus the discrete time lag m between these intensities. Recently, in the context of electrically coupled semiconductor chaotic lasers, cross-correlations have been considered, where the coexistence of both in-phase and antiphase patterns [50] was observed experimentally and numerically. In our system we clearly observe in Fig. 13(b) that for the coupling parameter $c = 0.0005$ in-phase and antiphase cross-correlations display a clear structure every time there is a delay difference $\Delta m \approx 8$. This behavior agrees

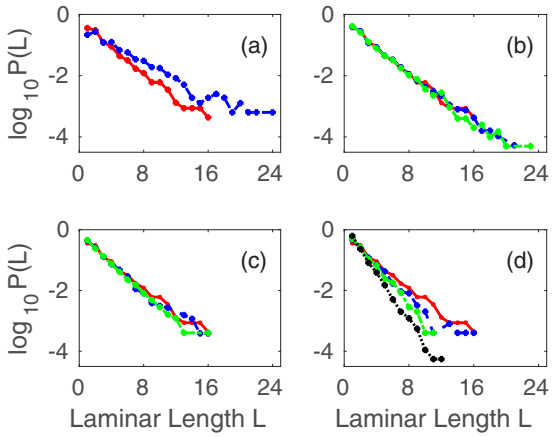

FIG. 12. PDF $P(L)$ for the laminar length L from a trajectory shadowing different UPOs with a given m. This is for the time series of I_1 given by the Poincaré section for different couplings c, when $Q = Q_1 = Q_2 = 2.26$. (a) $\log_{10} P(L)$ versus L for coupling constant $c = 0$ and $m = 8$ (red), $c = 0$ and $m = 9$ (blue). (b) Same as (a) for $m = 8$ when $c = 0.0002$ (blue), $c = 0.0005$ (green), and $c = 0$ (red). (c) Same as (a) for $m = 8$ when $c = 0.001$ (blue), $c = 0.0011$ (green), and $c = 0$ (red). (d) Same as (a) for $m = 8$ when $c = 0.0015$ (blue), $c = 0.002$ (green), $c = 0.003$ (black), and $c = 0$ (red). In panel (a) the steeper average slope corresponds to m = 8. In panel (d) the average slope becomes steeper as c increases.

with that for the AC in Fig. 11(b). For a weaker coupling, however, the CC pattern collapses as seen in Fig. 13(a) for $c = 0.00002$. In this case no ESARE is found in more than 10^5 consecutive iterations in the time series as shown in Fig. 4(a) and in practice both laser oscillators appear as uncoupled.

IV. ESARE AS EXCEPTIONAL N:N AND N:M RESONANCES

In this section we consider the origin of ESARE, as their main observable features were dealt with in the previous subsection, where we identified ESARE as local intensity

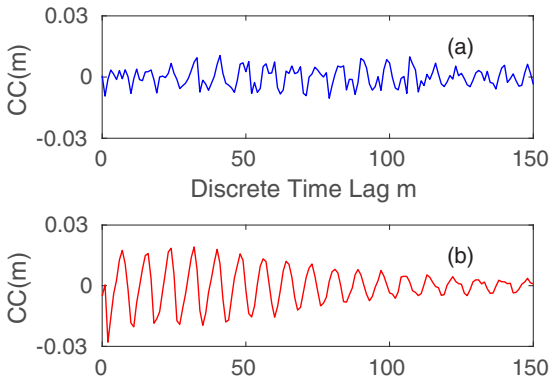

FIG. 13. Cross-correlation function for the dual discrete time series at the Poincaré section, which consists of the maxima of I_1 and the correspondig value for I_2, versus the discrete time lag m for two different coupling parameters c, when $Q = Q_1 = Q_2 = 2.26$. (a) The CC for the coupling parameter $c = 0.00002$. (b) Same as (a) but for $c = 0.0005$.

maxima $I_{1,2}$ when $I_{1,2} \ll 1$, i.e., below the undulations intensities, for coupling parameters $c \ll 1$. According to the model given by Eq. (1) it means that when one of the laser oscillators undergoes a spike, the intensity of the other laser oscillator reduces its effective decay rate (nonlinear losses) and therefore may have a local gain, which can result in an ESARE. This intuitive description has its origin or cause in the presence of certain resonances with small enough Floquet multipliers, which eventually are visited or shadowed by the trajectory. Below we provide evidence that these exceptional resonances are related to ESARE, and we give a short account on how to find them.

To develop insight into the solution structure, we explain it through a sequence of diagrams that together provide a brief account of the periodic solution families and their bifurcations. A more detailed report on this bifurcation structure will be considered elsewhere. In our bifurcation diagrams, solid (dashed) curves represent stable (unstable) solutions, respectively, Hopf bifurcations are shown as solid red squares, branch points as small open squares, and period-doubling bifurcations as open diamonds.

A. $N : N$ intermediate-phase resonances

Families of intermediate-phase periodic solutions of the coupled laser model can be computed quite systematically by numerical continuation. We have determined such families by coupling two identical solutions selected from an isola of the 3D single laser model. For small coupling constant c and varying Q such intermediate-phase families again take the form of isolas. To be more specific, the first step is to follow the phase-shift family for a fixed value of Q, for which we used $Q = 2.26$, along which the coupling constant c remains zero. Along this rather trivial family one encounters bifurcation points. For the standard 2D oscillator with quadratic nonlinearity it is known that the coupled 4D model, with linear coupling, has exactly two such bifurcations, namely one that leads to an in-phase family, and another one that leads to an antiphase family [51]. However, for the more general laser model that we consider here, the number of bifurcations from the phase-shift family can be more than two, and their precise number also depends on Q. Bifurcating families include the family of in-phase and the family of antiphase orbits, but in addition there are bifurcations that lead to families of intermediate-phase orbits.

We have applied this phase-shift continuation to two identical periodic solutions at $Q = 2.3$ from the isola $\hat{I}_{08}$ of the 3D laser model. These solutions are merged into one 6D solution of the coupled model, with coupling constant $c = 0$. During the phase-shift continuation the value of Q is kept fixed, while c and the period T are free continuation parameters, even though they actually remain constant, with $c = 0$. Several bifurcation points are encountered along the phase-shift family, in addition to those that lead to the in-phase and the antiphase families. Along such bifurcating families of intermediate-phase orbits we accurately locate target values of the coupling constant, for which we have used, for example, $c = 0.0005$ and $c = 0.0020$. Each of the corresponding intermediate-phase orbits was subsequently used as starting orbit for continuation with varying Q (and varying period T), while keeping c fixed. Although of considerable complexity,

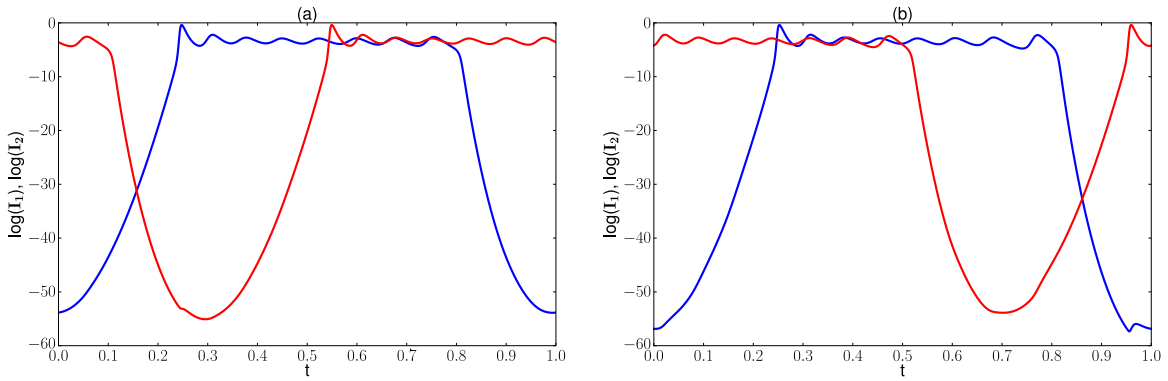

FIG. 14. Unstable resonances along two intermediate-phase isolas that arise from coupling two identical solutions of isola $\hat{I}_{08}$ of the single laser model. (a) $c = 0.0005$. (b) $c = 0.0020$. These resonances may give rise to ESARE in the trajectory. The coupled LSA have mirror symmetry.

the two resulting families are indeed isolas of intermediate-phase orbits, i.e., each family is represented by a closed curve in a bifurcation diagram. A selected orbit along each of the two isolas is shown in Fig. 14, on the left for an isola with $c = 0.0005$ and on the right for an isola with $c = 0.0020$. Their Floquet multipliers show that both solutions are only mildly unstable, while also possessing a strongly stable manifold.

B. $N : M$ resonances

Consider again the isolas of periodic orbits of the single laser model in Fig. 8, and in particular the isolas of periodic orbits represented there by a time-scaled L_2 norm as a function of Q. Now consider the alternate representation of these isolas shown in Figure 15, where instead of the L_2 norm the period of the orbits is used as vertical axis. Notice for example that the three curves representing the isolas $\hat{I}_{03}$, $\hat{I}_{04}$, and $\hat{I}_{05}$ (in black, red, and blue, respectively), intersect at various locations, as best seen in the panel on the right in Fig. 15. These intersection points correspond to *same-period resonances*, from which resonance zones known as Arnold tongues arise. We refer to these resonances using the indices of the corresponding isolas, for example, 03:04 for the resonance that arises from the intersection point of the isolas $\hat{I}_{03}$ and $\hat{I}_{04}$ near the left-hand folds in Fig. 15. There are also resonance zones that correspond to rational resonances, but these we do not consider here. Also note that referring to resonance points as, for example, 03:04, is perhaps somewhat misleading, as they are actually same-period resonances.

For any given resonance, say, 06:07, we take the two resonant orbits, one from from $\hat{I}_{06}$, and the other from $\hat{I}_{07}$, both having the same period and the same value of Q. Starting from $c = 0$, the combined 6D orbit can generally be continued in c, keeping Q fixed. Since at $c = 0$ the two lasers are uncoupled, they can also be phase shifted relative to each other. Such phase-shifted solutions can also be continued in c. Due to the complexity of the ensuing two-dimensional (2D) manifold of solutions, some of such phase-shifted solution can be continued to larger values of c than others, while keeping Q fixed. Practically a search is needed over various phase shifts at $c = 0$ in order to continue to a desired target value of c. Such a search has been carried out successfully for many resonances to provide starting orbits at $c = 0.0015$.

Subsequent continuation of the starting solutions at $c = 0.0015$, keeping c fixed and allowing Q to vary, produces isolas of periodic orbits. A selected fold along such an isola can be followed with varying c, to provide a starting solution (at a fold) for other selected values of c. As examples, the

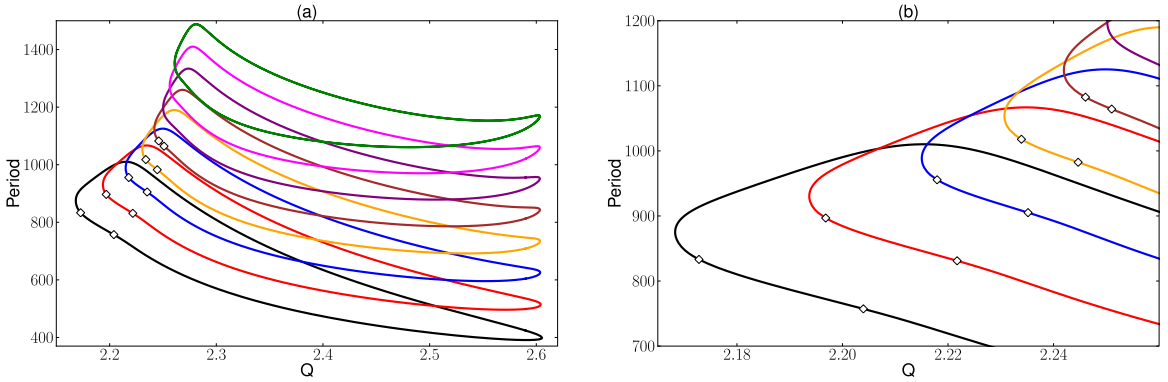

FIG. 15. (a) Another representation of the isolas $\hat{I}_{03}$–$\hat{I}_{10}$ from Fig. 8 with Q as free parameter, now with the period T as vertical axis. Only solid curves are used, even though the only stable regions are between the period-doubling bifurcations (open diamonds) along the isolas $\hat{I}_{03}$–$\hat{I}_{07}$. (b) A detail of the diagram on the left. The smallest period T near the fold at $Q \approx 2.6$ corresponds to isola $\hat{I}_{03}$, the next fold to $\hat{I}_{04}$, and so on.

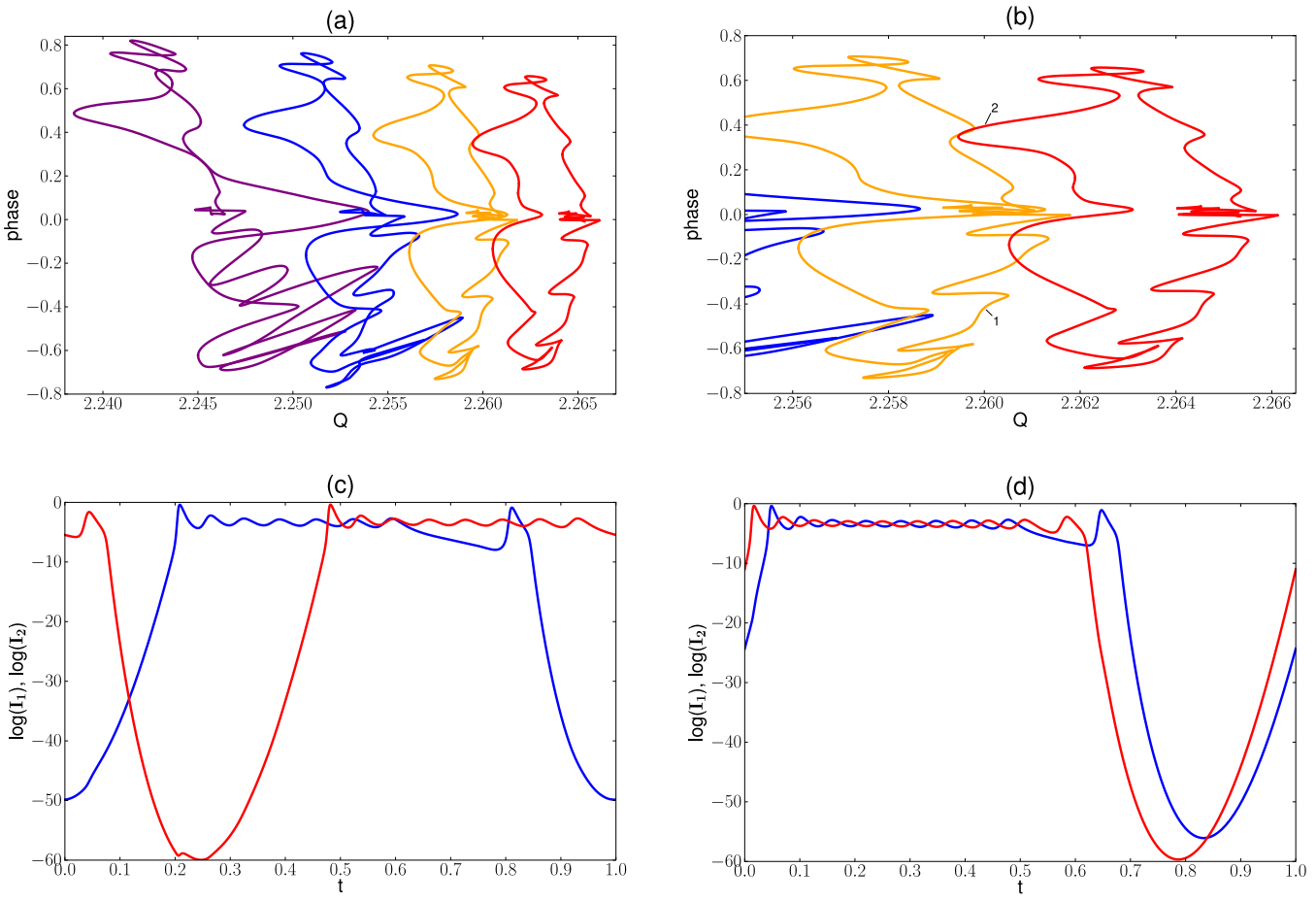

FIG. 16. (a) Phase integral versus Q for, from left to right, the isolas $\hat{I}_{06:07}$ (purple), $\hat{I}_{07:08}$ (blue), $\hat{I}_{08:09}$ (orange), and $\hat{I}_{09:10}$ (red), for $c = 0.0020$. (b) A detail of panel (a). (c) The resonance labeled 1 in panel (b). (d) The resonance labeled 2 in panel (b). The coupled LSA have mirror symmetry.

isolas $\hat{I}_{06:07}$, $\hat{I}_{07:08}$, $\hat{I}_{08:09}$, and $\hat{I}_{09:10}$ at $c = 0.0005$ are shown in the top-left panel of Fig. 16, where a phase integral is used as vertical axis. Note that the solution shown in the bottom-left panel is from the isola $\hat{I}_{08:09}$ (orange), with 8 maxima for laser 1 (blue) and 9 maxima for laser 2, not counting the local maximum of laser 2 (a "rare event") near the bottom of that panel. Similarly, the bottom-right panel shows a solution along the isola $\hat{I}_{09:10}$ (red), with 9 maxima for laser 1 (blue) and 10 maxima for laser 2 (red). The numerous folds along the isolas can be continued in the parameters Q, c, and the period T, in order to provide an impression of the shape of the resonance zones for these isolas. Solutions along the $N : M$ isolas in this section are generally highly unstable.

V. CASE II: EXTREME RARE EVENTS IN ASYMMETRICALLY PUMPED LASER OSCILLATORS

In the present section we consider a different setting for the pair of mutually coupled lasers, where we now show evidence of extreme rare events or rogue waves when, as in the previous case, the coupling parameter is much smaller than the threshold for chaotic synchronization c_{sync}. However, in this case the coupled lasers have an asymmetric configuration: the laser pump parameter in both laser oscillators are different near a Hopf bifurcation.

To be more precise, near the in-phase Hopf bifurcation (HBI) in Fig. 17, which stands for the case of the symmetrically coupled laser oscillators of the previous section, we introduce an asymmetry in Eq. (1), i.e., by slightly perturbing the lasers pump parameters such that $Q_1 < Q_{\text{HBI}}$, $Q_2 > Q_{\text{HBI}}$.

As the solution to the right of Q_{HBI} is the stable steady state with $I_1 = I_2$, and that of the left is a chaotic attractor, as suggested by Fig. 18, simulations and numerical continuation, the typical solution for this asymmetric setting becomes a perturbation arising from the uncoupled chaotic solution and the steady state for I_1 and I_2, respectively, as long as the coupling parameter c is small enough: $c \ll c_{\text{sync}}$.

The continuous time evolution in this configuration for $\log(I_1)$ and $\log(I_2)$ is shown in Fig. 18, where a single event displaying a RW is observed in the time series for I_2. The laser intensity I_1 qualitatively behaves as in the absence of coupling, in contrast I_2 eventually displays bursts from a characteristic stationary solution near a steady state. These bursts consist of spikes each of which is followed by several undulations, as also seen in the previous section when $Q_1 = Q_2$, for very small coupling c: $c \ll c_{\text{sync}}$. Moreover, when a RW occurs in I_2, a few ESARE may develop as well, although not shown explicitly in these time series, ESARE appear in the PDF for the statistics of the maxima of $\log(I_2)$ as shown below.

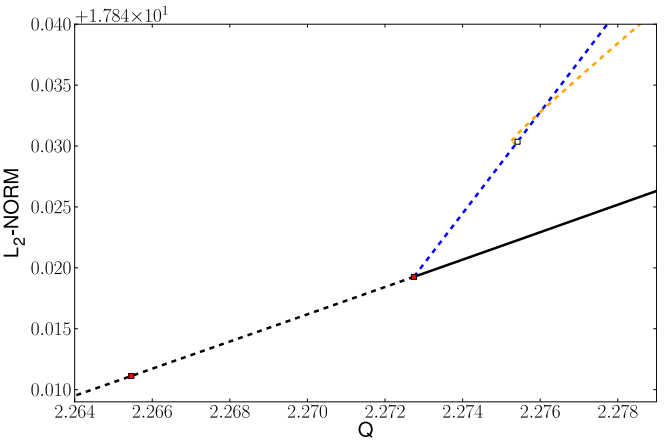

FIG. 17. $c = 0.005$. The curve that contains the two small solid squares (Hopf bifurcations) represents nonzero stationary states. A family of antiphase periodic solutions (not shown) bifurcates from the Hopf point on the left. Shown is a family of in-phase periodic solutions that bifurcates from the Hopf point on the right, as well as an intermediate-phase family that bifurcates from the in-phase family at the point marked by a small open square.

Figure 19 is a detail of Fig. 18 which suggests a more complicated structure for resonances related to RW in the evolution of $\log(I_2)$.

Figure 20(a) is a detail of Fig. 18, which shows the behavior of $\log(I_2)$ just before a RW develops. Rogue wave prediction is an important issue, and in optical systems it was discussed and reported in several articles [9,10,12]. Recent articles discuss RW prediction for a loss modulated CO_2 laser model [52,53]. In our case we observe that a monotonic nondecreasing almost regular oscillations for $\log(I_2)$ develop, which eventually goes beyond a certain threshold for $\log(I_2)$ and becomes a RW. By a similar token a RW comes to an end with monotonic decreasing almost regular oscillations as seen in Fig. 20(b).

In the absence of RW, the characteristic behavior of $\log(I_2)$ is composed of rapid oscillations whose amplitude is slowly modulated in a stochastic fashion as suggested by Fig. 21(b),

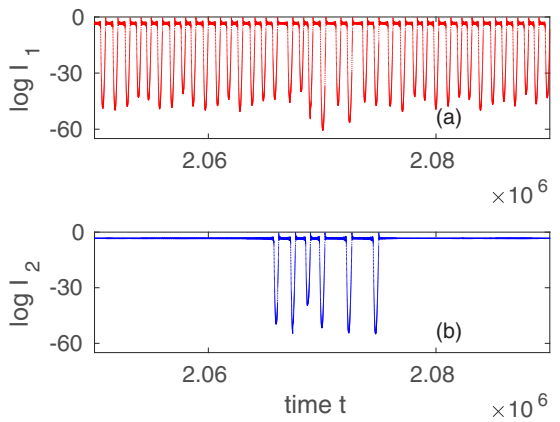

FIG. 18. Continuous time series for $\log(I_1)$ and $\log(I_2)$ shown in (a) and (b), respectively. The coupling parameter is $c = 0.005$, and $Q_1 = 2.27$, $Q_2 = 2.2835$. Here a single rare event is shown. $\log I_{1,2} \equiv \ln I_{1,2}$. Here log denotes natural logarithm.

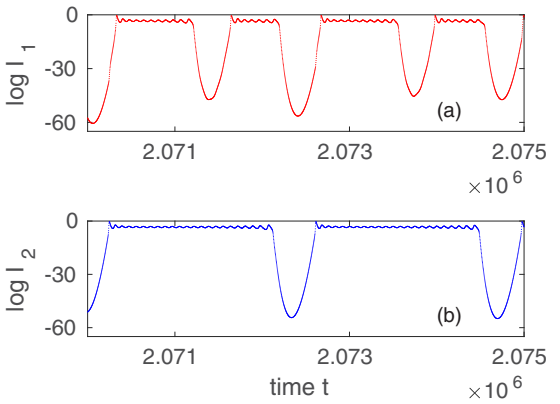

FIG. 19. Detail of Fig. 18, which suggests the presence of complex resonances when a rare event happens.

while in Fig. 21(a) $\log(I_1)$ behaves qualitatively as in the absence of coupling.

To appreciate better the rise of a RW in I_2 from the background of stochastic stationary oscillations localized around the steady state solution for $Q_1 = Q_2$, we plot $I_2 \geqslant \exp(-3.5)$ as Q_2 increases from Q_{HBI} in the three panels of Fig. 22. In Fig. 22(c) $Q_2 = 2.285$ is too large to observe any rare event during the sampled time, while in Fig. 22(a) many large amplitude events are observed. In between these opposite behaviors, Fig. 22(b) appears as appropriate to suggest the presence of RW in I_2, as in a sample consisting of 10^6 Poincaré map successive iterates RW emerge less than fifty times.

In Fig. 23(a) a PDF is shown for the discrete time series consisting of maxima for I_2 for data points when $I_2 \geqslant \exp(-3.5)$. This amounts to almost all data sets, approximately 1.2×10^6, where rogue waves are eventually observed. The red (blue) points stand for an interval partition in the histogram with $\Delta = 0.25$ ($\Delta = 0.50$). The observed rare events in the complete time series for I_2 consist of both ESARE and RW. For the sake of clarity and resolution we also display the PDF for $I_2 < \exp(-3.5)$ in Fig. 23(b), where the data set has just 119 points. In Fig. 23(a) one may argue that the PDF for $\exp(-3.5) < I_2 < \exp(-1.5)$ suggests a power law, while the RW itself is a clear-cut outlier where $I_2 \sim \exp(-0.5)$.

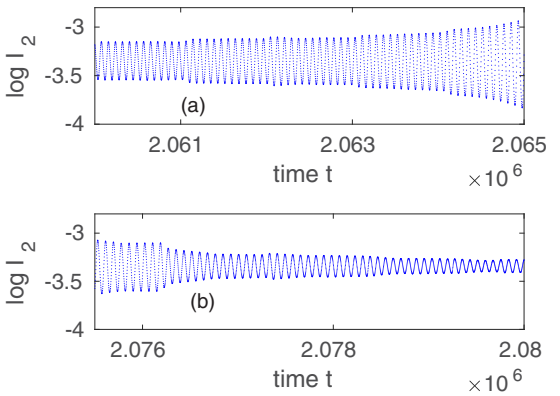

FIG. 20. Detail of Fig. 18, which shows the behavior of the time series for $\log(I_2)$ just before (a) and soon after (b) a rare event occurred.

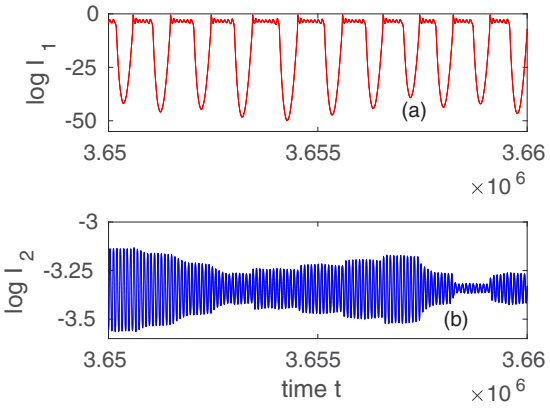

FIG. 21. Detail of Fig. 18, which shows the behavior of the characteristic time series for $\log(I_2)$ in the absence of any rare event.

In addition to the PDF, also of interest is the estimation of the AC for the discrete time series of I_2 shown in Fig. 22. Figure 24 evaluates the AC for different values of Q_2 when $Q_1 = 2.27$ and the coupling parameter $c = 0.005$ are kept constant. As Q_2 increases, the AC tail becomes shorter for larger discrete time delay m when compared to that of Fig. 24(a) for $Q_2 = 2.283$. This is seen in Figs. 24(b), 24(c) and 24(d) where the AC tails fluctuate. In addition, in Fig. 24(d) for $Q_2 = 2.285$ the AC tail collapses to a very small value of the order of the fluctuation for a random signal, whose order behaves as $\frac{1}{\sqrt{N}}$, where N is the size of the data set [48], $N \approx 10^6$. The observed fluctuations in the AC are the result of the relative correlation between the undulations before and after the spikes in the discrete time series of I_2. As Q_2 increases the undulations become modulated in an almost random fashion during longer time intervals and bursts become more unusual, as observed in panel (b) of Fig. 21. The result is the collapse of the AC as shown in Fig. 21(d).

As in the symmetric configuration case, the CC is evaluated for the dual time series [48], which this time consists of data at

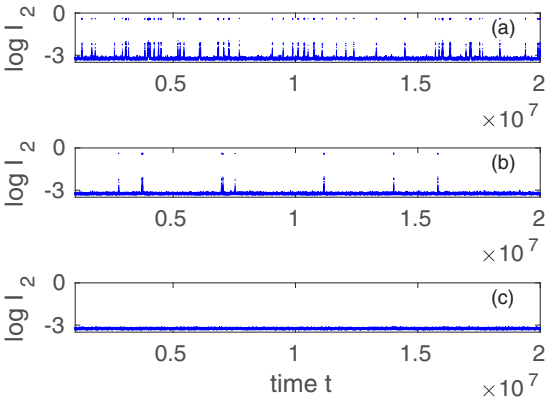

FIG. 22. Time series for the Poincaré section from the maxima of I_2 in Eq. (1) for the coupling constant $c = 0.005$, pump parameter $Q_1 = 2.27$, and $Q_2 = 2.283$ (a), $Q_2 = 2.284$ (b), and $Q_2 = 2.285$ (c). Here the number of iterates for the Poincaré section is of the order of 10^5 in each panel, and only $I_2 \geqslant \exp(-3.5)$ is considered for the sake of resolution. Here log denotes natural logarithm.

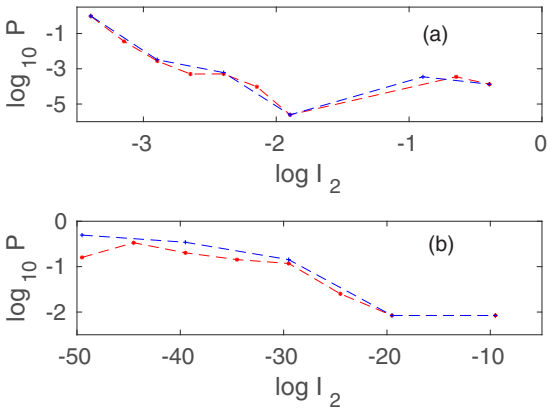

FIG. 23. PDF for the time series consisting of maxima for I_2 when $Q_1 = 2.27$, $Q_2 = 2.284$, and coupling parameter $c = 0.005$. (a) For data points when $I_2 \geqslant \exp(-3.5)$, which amount to almost all data, approximately 1.2×10^6, where rogue waves are eventually observed. The red (blue) points stand for an interval partition of $\Delta = 0.25$ ($\Delta = 0.50$) in the histogram. (b) PDF for data points when $I_2 < \exp(-3.5)$, which amount to 119, where ESARE are observed. The red (blue) points stand for an interval partition of $\Delta = 5$ ($\Delta = 10$) in the histogram. Here log denotes natural logarithm.

the Poincaré section for the maxima of I_2 and the related value of I_1, versus the discrete time lag m between these intensities. The Poincaré section is chosen to be the maxima of I_2 as the RW occur in the time series for I_2.

In this configuration we clearly observe in Fig. 25(a) that antiphase cross-correlations are dominant for the most part of m, except when $m = 0$, for the three different time series shown in Fig. 22. Here the coupling parameter is $c = 0.005$. When $Q_2 = 2.285$ there are no bursts in the time series for I_2. Here in spite of regular continuous undulations whose amplitude displays slow random modulations as observed in

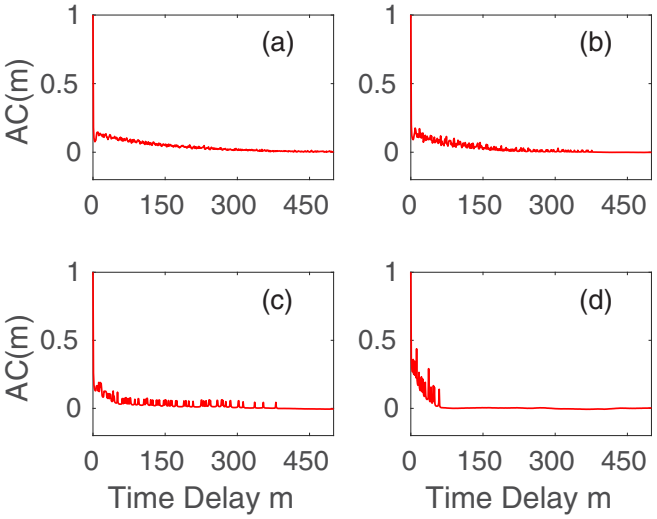

FIG. 24. The AC for the time series consisting of the maxima of I_2 versus the discrete time delay m for different parameters Q_2 when $Q_1 = 2.27$ and $c = 0.005$. (a) The AC for the pump parameter $Q_2 = 2.283$. (b) Same as (a) but for $Q_2 = 2.284$. (c) Same as (a) but for $Q_2 = 2.2845$. (d) Same as (a) but for $Q_2 = 2.285$.

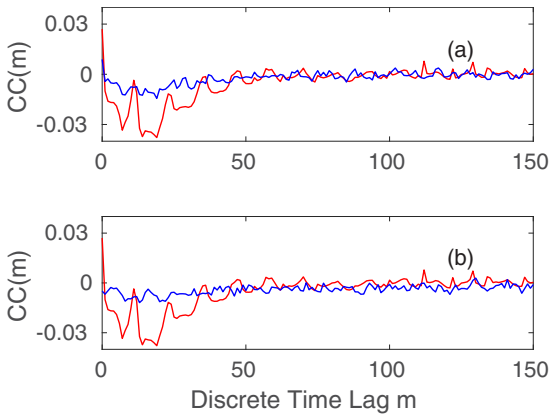

FIG. 25. Cross-correlation function for the dual discrete time series at the Poincaré section, which consists of the maxima of I_2 and the corresponding value for I_1, versus the discrete time lag m for different parameters Q_2, when $Q_1 = 2.27$ and $c = 0.005$. (a) The CC versus m for the pump parameters $Q_2 = 2.285$ (red) and $Q_2 = 2.284$ (blue). (b) Same as (a) but for the pump parameters $Q_2 = 2.285$ (red) and $Q_2 = 2.283$ (blue). The largest antisymmetric cross-correlations arise when the pump equals 2.285.

Fig. 21(b), the CCs between I_2 and I_1 show clear antiphase correlations as observed in Fig. 25(a) for $Q_2 = 2.285$. For $Q_2 = 2.283$ and $Q_2 = 2.284$ the antiphase correlations decrease, and bursts are more frequent for $Q_2 = 2.283$ than for $Q_2 = 2.284$.

VI. CONCLUSIONS AND DISCUSSION

We have studied rare events of two kinds corresponding to symmetric and asymmetric configurations in a model for a pair of weakly coupled lasers, which when uncoupled show mixed-mode oscillations (MMO) and chaos with one fast variable and two slow variables. The rare events with an extremely small amplitude (ESARE) arise in the symmetric laser configuration and its rate of occurrence depending on the coupling constant has been studied. We analysed its statistics, where a characteristic power law develops for the histogram of the laser intensities from ESARE. Symbolic dynamics, using as partition the number of maxima of the embedded UPOs in the attractor, allows for determination of the components of the resonances for very weak coupling. This was useful as a starting point to find the origin of ESARE, whose genesis is related to the presence of $N : M$ intermediate-phase resonances, such as $N : M = 8 : 8$, $9 : 9$, $8 : 9$, and so on. These resonances are built up from pairs of periodic orbits which belong to Isolas for the uncoupled system, where the relative phase between these periodic orbits, mostly UPOs, is suitably shifted until a bifurcation is found. In a second step, numerical continuation is carried out having as free parameters the coupling strenght and laser pump.

The second rare event considered in our study is a rogue wave. This arises in the asymmetric laser configuration for small enough coupling parameter, when the pump parameters in both laser oscillators are different near an in-phase Hopf bifurcation. The laser oscillator having its pump parameter, its control, larger than that for the in-phase Hopf bifurcation exhibits rogue waves whose rate of occurrence depending on its control has been studied. We believe that more complex resonances are at the origin of the observed RW, as suggested by our study of ESARE, which are generated by exceptional $N : M$ and $N : N$ resonances. We defer the study of the RW resonances for future work as the codimension in this analysis is higher. We found that the related precursors are oscillations with an almost similar period and predominantly with slowly fluctuating amplitudes. In a model for the loss modulated CO_2 laser, precursors have been associated with certain UPOs [52], and the time spent by the trajectory near a singular point [53]. In low-dimensional chaotic laser models RW were found to be induced by crises [52]; however, in our coupled system RW arise near an in-phase Hopf bifurcation, where intermittency arises between a fluctuating state, near a stationary solution and a MMO of the laser system, which we associate with certain UPOs, special resonances. The typical amplitude of the RW is about 20 times larger than the average and standard deviation of the fluctuating state amplitude: The RW appear as large isolated spikes over an almost regular backround. In the context of a master-slave coupled system within the bubbling dynamical regime, histograms of extreme rare events do not follow the typical power-law behavior [54]. The related outliers were identified as dragon kings, as these possess distinct formation mechanisms. A recent case of these outliers in optics was reported within the context of random laser emission [55]. In our system the corresponding histograms for the asymmetric case indicate that the mechanism for the genesis of the outliers is the presence of special resonances, as suggested by our study of ESARE. A detailed study of the latter is left for future work.

We also considered autocorrelation and cross-correlation functions for the time series of ESARE and the RW. Here clear patterns are found where in-phase and antiphase cross-correlations emerge. This suggests that certain sequences of resonances are more likely to be visited or shadowed by the trajectory in spite of the very weak coupling strength. The latter is weak when compared to that for complete synchronization.

As the interaction between the laser oscillators in our model, Eq. (1), is given via inhibitory nonlinear coupling, we think that certain models of neurons, such as those for central pattern generators described by Hodgkin-Huxley models [56], may exhibit rare events qualitatively similar to those presented in this study. Moreover, due to the ubiquity of MMO in science, we expect similar rare events to be found in other experimental settings and in applications.

ACKNOWLEDGMENTS

This work was supported by NSERC (Canada), BUAP (México), and CONACYT (México).

[1] S. Albeverio, V. Jentsch, and H. Kantz H. (eds.), *Extreme Events in Nature and Society* (Springer, Berlin, 2006).

[2] A. D. Donnenberg and V. S. Donnenberg, Clin. Lab. Med. **27**, 627 (2007).

[3] F. Dyson, *Disturbing the Universe* (Basic Books Inc., New York, 1979).

[4] N. N. Taleb, *The Black Swan* (Random House, New York, 2007).

[5] M. Ghil, P. Yiou, S. Hallegatte *et al.*, Nonlin. Process. Geophys. **18**, 295 (2011).

[6] D. Sornette, *Critical Phenomena in Natural Sciences* (Springer-Verlag, Berlin, 2007).

[7] A. D. Cattrell, M. Srokosz, B. I. Moat, and R. Marsh, Sci. Rep. **9**, 4461 (2019).

[8] D. R. Solli, C. Ropers, P. Koonath, and B. Jalali, Nature **450**, 1054 (2007).

[9] C. Bonatto, M. Feyereisen, S. Barland, M. Giudici, C. Masoller, Jose R. Rios Leite, and J. R. Tredicce, Phys. Rev. Lett. **107**, 053901 (2011).

[10] N. Akhmediev, B. Kibler, F. Baronio *et al.*, J. Opt. **18**, 063001 (2016).

[11] E. Mercier, A. Even, E. Mirisola, D. Wolfersberger, and M. Sciamanna, Phys. Rev. E **91**, 042914 (2015).

[12] J. Zamora-Munt, B. Garbin, S. Barland, M. Giudici, Jose R. Rios Leite, C. Masoller, and J. R. Tredicce, Phys. Rev. A **87**, 035802 (2013); C. Metayer, A. Serres, E. J. Rosero, W. A. S. Barbosa, F. M. de Aguiar, J. R. Rios Leite, and J. R. Tredicce, Opt. Express **22**, 19850 (2014); N. M. Granese, A. Lacapmesure, M. B. Agüero, M. G. Kovalsky, A. A. Hnilo, and J. R. Tredicce, Opt. Lett. **41**, 3010 (2016).

[13] V. S. L'vov, A. Pomyalov, and I. Procaccia, Phys. Rev. E **63**, 056118 (2001).

[14] M. Rivera, G. Martinez Mekler, and P. Parmananda, Chaos **16**, 037105 (2006).

[15] S. Boccaletti, A. N. Pisarchik, C. I. del Genio, and A. Amann, *Synchronization: From Coupled Systems to Complex Networks* (Cambridge University Press, Cambridge, 2018).

[16] S. K. Han, C. Kurrer, and Y. Kuramoto, Phys. Rev. Lett. **75**, 3190 (1995).

[17] M. A. Harrison, Y.-Ch. Lai, and R. D. Holt, Phys. Rev. E **63**, 051905 (2001).

[18] K. S. Thornburg, Jr., M. Moller, R. Roy, T. W. Carr, R. D. Li, and T. Erneux, Phys. Rev. E **55**, 3865 (1997).

[19] P. Ashwin, J. R. Terry, K. S. Thornburg, Jr., and R. Roy, Phys. Rev. E **58**, 7186 (1998).

[20] C. Masoller, H. L. D. de S. Cavalcante, and J. R. Rios Leite, Phys. Rev. E **64**, 037202 (2001).

[21] I. Z. Kiss, V. Gaspar, and J. L. Hudson, J. Phys. Chem. B **104**, 7554 (2000).

[22] J. Zamora-Munt, C. Masoller, and J. Garcia-Ojalvo, and R. Roy, Phys. Rev. Lett. **105**, 264101 (2010).

[23] P. Ashwin, J. Buescu, and I. Stewart, Phys. Lett. A **193**, 126 (1994).

[24] J. F. Heagy, T. L. Carroll, and L. M. Pecora, Phys. Rev. Lett. **73**, 3528 (1994).

[25] V. Astakhov, A. Shabunin, T. Kapitaniak, and V. Anishchenko, Phys. Rev. Lett. **79**, 1014 (1997).

[26] M. Brons, T. J. Kaper, and H. G. Rotstein, Chaos **18**, 015101 (2008).

[27] M. Desroches, J. Guckenheimer, B. Krauskopf, Ch. Kuehn, H. M. Osinga, and M. Wechselberger, SIAM Rev. **54**, 211 (2012).

[28] J. Guckenheimer and C. Scheper, SIAM J. Appl. Dynam. Syst. **10**, 92 (2011); J. G. Freire and J. A. C. Gallas, Phys. Lett. A **375**, 1097 (2011); N. Baba and K. Krisher, Chaos **18**, 015103 (2008); M. Desroches, B. Krauskopf, and H. M. Osinga, *ibid.* **18**, 015107 (2008).

[29] N. B. Abraham, P. Mandel, L. M. Narducci, Prog. Opt. **25**, 1 (1988).

[30] T. Erneux and P. Glorieux, *Laser Dynamics* (Cambridge University Press, New York, 2010).

[31] P. Mandel, *Theoretical Problems in Cavity Nonlinear Optics* (Cambridge University Press, New York, 2005).

[32] A. Barsella, C. Lepers, D. Dangoisse, P. Glorieux, and T. Erneux, Opt. Commun. **165**, 251 (1999).

[33] T. Sugawara, M. Tachikawa, T. Tsukamoto, and T. Shimizu, Phys. Rev. Lett. **72**, 3502 (1994).

[34] I. Susa, T. Erneux, A. Barsella, C. Lepers, D. Dangoisse, and P. Glorieux, Phys. Rev. A **63**, 013815 (2000).

[35] E. J. Doedel, B. E. Oldeman *et al.*, *AUTO-07P: Continuation and Bifurcation Software for Ordinary Differential Equations* (Concordia University, Montréal, 2011).

[36] E. J. Doedel, B. E. Oldeman, and C. L. Pando L., Int. J. Bifurcat. Chaos **21**, 305 (2011).

[37] E. J. Doedel, and C. L. Pando L., Int. J. Bifurcat. Chaos **22**, 1250238 (2012).

[38] M. Tachikawa, F. L. Hong, K. Tanii, and T. Shimizu, Phys. Rev. Lett. **60**, 2266 (1988); M. Tachikawa, K. Tanii, and T. Shimizu, J. Opt. Soc. Am. B **5**, 1077 (1988).

[39] D. Hennequin, F. de Tomasi, B. Zambon, and E. Arimondo, Phys. Rev. A **37**, 2243 (1988).

[40] D. Dangoisse, A. Bekkali, F. Pappof, and P. Glorieux, Europhys. Lett. **6**, 335 (1988).

[41] M. Lefranc, D. Hennequin, and D. Dangoisse, J. Opt. Soc. Am. B **8**, 239 (1991).

[42] V. V. Nevdakh, O. L. Gaiko, and L. N. Orlov, Opt. Commun. **127**, 303 (1996).

[43] H. L. D. de S. Cavalcante, and J. R. Rios Leite, Chaos **18**, 023107 (2008).

[44] E. J. Doedel, and Carlos L. Pando L., Phys. Rev. E **89**, 052904 (2014).

[45] E. J. Doedel, and C. L. Pando L., Eur. Phys. J.: Spec. Top. **226**, 467 (2017).

[46] E. J. Doedel, and C. L. Pando L., Eur. Phys. J.: Spec. Top. **225**, 2613 (2016).

[47] E. J. Doedel, B. Krauskopf, and C. L. Pando L., Eur. Phys. J. Spec. Top. **223**, 2847 (2014).

[48] C. Chatfield, *The Analysis of Time Series: Theory and Practice* (Chapman & Hall, London, 1975).

[49] R. Meucci, F. Salvadori, M. V. Ivanchenko, K. A. Naimee, C. Zhou, F. T. Arecchi, S. Boccaletti, and J. Kurths, Phys. Rev. E **74**, 066207 (2006).

[50] E. J. Rosero, W. A. S. Barbosa, J. F. Martinez Avila, A. Z. Khoury, and J. R. Rios Leite, Phys. Rev. E **94**, 032210 (2016).

[51] D. G. Aronson, E. J. Doedel, and H. G. Othmer, Physica D **25**, 20 (1987).

[52] C. Bonatto and A. Endler, Phys. Rev. E **96**, 012216 (2017).

[53] S. Kumarasamy and A. N. Pisarchik, Phys. Rev. E **98**, 032203 (2018).

[54] H. L. D. de S. Cavalcante, M. Oria, D. Sornette, E. Ott, and D. J. Gauthier, Phys. Rev. Lett. **111**, 198701 (2013).

[55] F. Tommasi, L. Fini, E. Ignesti, S. Lepri, F. Martelli, and S. Cavalieri, Phys. Rev. A **98**, 053816 (2018).

[56] N. Kopell and G. B. Ermentrout, in *Handbook of Dynamical Systems*, Vol. 2, edited by B. Fiedler (Elsevier, Amsterdam, 2002), pp. 3–54; F. Skinner, N. Kopell, and E. Marder, J. Comput. Neurosci. **1**, 69 (1994); E. Marder and R. L. Calabrese, Phys. Rev. **76**, 687 (1996).